Search for long-lived gravitational-wave transients coincident with long gamma-ray bursts

J. Aasi,[1] J. Abadie,[1] B. P. Abbott,[1] R. Abbott,[1] T. Abbott,[2] M. R. Abernathy,[1] T. Accadia,[3] F. Acernese,[4,5] C. Adams,[6] T. Adams,[7] R. X. Adhikari,[1] C. Affeldt,[8] M. Agathos,[9] N. Aggarwal,[10] O. D. Aguiar,[11] P. Ajith,[1] B. Allen,[8,12,13] A. Allocca,[14,15] E. Amador Ceron,[12] D. Amariutei,[16] R. A. Anderson,[1] S. B. Anderson,[1] W. G. Anderson,[12] K. Arai,[1] M. C. Araya,[1] C. Arceneaux,[17] J. Areeda,[18] S. Ast,[13] S. M. Aston,[6] P. Astone,[19] P. Aufmuth,[13] C. Aulbert,[8] L. Austin,[1] B. E. Aylott,[20] S. Babak,[21] P. T. Baker,[22] G. Ballardin,[23] S. W. Ballmer,[24] J. C. Barayoga,[1] D. Barker,[25] S. H. Barnum,[10] F. Barone,[4,5] B. Barr,[26] L. Barsotti,[10] M. Barsuglia,[27] M. A. Barton,[25] I. Bartos,[28] R. Bassiri,[29,26] A. Basti,[14,30] J. Batch,[25] J. Bauchrowitz,[8] Th. S. Bauer,[9] M. Bebronne,[3] B. Behnke,[21] M. Bejger,[31] M. G. Beker,[9] A. S. Bell,[26] C. Bell,[26] I. Belopolski,[28] G. Bergmann,[8] J. M. Berliner,[25] D. Bersanetti,[32,33] A. Bertolini,[9] D. Bessis,[34] J. Betzwieser,[6] P. T. Beyersdorf,[35] T. Bhadbhade,[29] I. A. Bilenko,[36] G. Billingsley,[1] J. Birch,[6] M. Bitossi,[14] M. A. Bizouard,[37] E. Black,[1] J. K. Blackburn,[1] L. Blackburn,[38] D. Blair,[39] M. Blom,[9] O. Bock,[8] T. P. Bodiya,[10] M. Boer,[40] C. Bogan,[8] C. Bond,[20] F. Bondu,[41] L. Bonelli,[14,30] R. Bonnand,[42] R. Bork,[1] M. Born,[8] V. Boschi,[14] S. Bose,[43] L. Bosi,[44] J. Bowers,[2] C. Bradaschia,[14] P. R. Brady,[12] V. B. Braginsky,[36] M. Branchesi,[45,46] C. A. Brannen,[43] J. E. Brau,[47] J. Breyer,[8] T. Briant,[48] D. O. Bridges,[6] A. Brillet,[40] M. Brinkmann,[8] V. Brisson,[37] M. Britzger,[8] A. F. Brooks,[1] D. A. Brown,[24] D. D. Brown,[20] F. Brückner,[20] T. Bulik,[49] H. J. Bulten,[9,50] A. Buonanno,[51] D. Buskulic,[3] C. Buy,[27] R. L. Byer,[29] L. Cadonati,[52] G. Cagnoli,[42] J. Calderón Bustillo,[53] E. Calloni,[4,54] J. B. Camp,[38] P. Campsie,[26] K. C. Cannon,[55] B. Canuel,[23] J. Cao,[56] C. D. Capano,[51] F. Carbognani,[23] L. Carbone,[20] S. Caride,[57] A. Castiglia,[58] S. Caudill,[12] M. Cavaglià,[17] F. Cavalier,[37] R. Cavalieri,[23] G. Cella,[14] C. Cepeda,[1] E. Cesarini,[59] R. Chakraborty,[1] T. Chalermsongsak,[1] S. Chao,[60] P. Charlton,[61] E. Chassande-Mottin,[27] X. Chen,[39] Y. Chen,[62] A. Chincarini,[32] A. Chiummo,[23] H. S. Cho,[63] J. Chow,[64] N. Christensen,[65] Q. Chu,[39] S. S. Y. Chua,[64] S. Chung,[39] G. Ciani,[16] F. Clara,[25] D. E. Clark,[29] J. A. Clark,[52] F. Cleva,[40] E. Coccia,[66,67] P.-F. Cohadon,[48] A. Colla,[19,68] M. Colombini,[44] M. Constancio, Jr.,[11] A. Conte,[19,68] R. Conte,[69] D. Cook,[25] T. R. Corbitt,[2] M. Cordier,[35] N. Cornish,[22] A. Corsi,[70] C. A. Costa,[11] M. W. Coughlin,[71] J.-P. Coulon,[40] S. Countryman,[28] P. Couvares,[24] D. M. Coward,[39] M. Cowart,[6] D. C. Coyne,[1] K. Craig,[26] J. D. E. Creighton,[12] T. D. Creighton,[34] S. G. Crowder,[72] A. Cumming,[26] L. Cunningham,[26] E. Cuoco,[23] K. Dahl,[8] T. Dal Canton,[8] M. Damjanic,[8] S. L. Danilishin,[39] S. D'Antonio,[59] K. Danzmann,[8,13] V. Dattilo,[23] B. Daudert,[1] H. Daveloza,[34] M. Davier,[37] G. S. Davies,[26] E. J. Daw,[73] R. Day,[23] T. Dayanga,[43] R. De Rosa,[4,54] G. Debreczeni,[74] J. Degallaix,[42] W. Del Pozzo,[9] E. Deleeuw,[16] S. Deléglise,[48] T. Denker,[8] T. Dent,[8] H. Dereli,[40] V. Dergachev,[1] R. DeRosa,[2] R. DeSalvo,[69] S. Dhurandhar,[75] L. Di Fiore,[4] A. Di Lieto,[14,30] I. Di Palma,[8] A. Di Virgilio,[14] M. Díaz,[34] A. Dietz,[17] K. Dmitry,[36] F. Donovan,[10] K. L. Dooley,[8] S. Doravari,[6] M. Drago,[76,77] R. W. P. Drever,[78] J. C. Driggers,[1] Z. Du,[56] J.-C. Dumas,[39] S. Dwyer,[25] T. Eberle,[8] M. Edwards,[7] A. Effler,[2] P. Ehrens,[1] J. Eichholz,[16] S. S. Eikenberry,[16] G. Endrőczi,[74] R. Essick,[10] T. Etzel,[1] K. Evans,[26] M. Evans,[10] T. Evans,[6] M. Factourovich,[28] V. Fafone,[59,67] S. Fairhurst,[7] Q. Fang,[39] S. Farinon,[32] B. Farr,[79] W. Farr,[79] M. Favata,[80] D. Fazi,[79] H. Fehrmann,[8] D. Feldbaum,[16,6] I. Ferrante,[14,30] F. Ferrini,[23] F. Fidecaro,[14,30] L. S. Finn,[81] I. Fiori,[23] R. Fisher,[24] R. Flaminio,[42] E. Foley,[18] S. Foley,[10] E. Forsi,[6] N. Fotopoulos,[1] J.-D. Fournier,[40] S. Franco,[37] S. Frasca,[19,68] F. Frasconi,[14] M. Frede,[8] M. Frei,[58] Z. Frei,[82] A. Freise,[20] R. Frey,[47] T. T. Fricke,[8] P. Fritschel,[10] V. V. Frolov,[6] M.-K. Fujimoto,[83] P. Fulda,[16] M. Fyffe,[6] J. Gair,[71] L. Gammaitoni,[44,84] J. Garcia,[25] F. Garufi,[4,54] N. Gehrels,[38] G. Gemme,[32] E. Genin,[23] A. Gennai,[14] L. Gergely,[82] S. Ghosh,[43] J. A. Giaime,[2,6] S. Giampanis,[12] K. D. Giardina,[6] A. Giazotto,[14] S. Gil-Casanova,[53] C. Gill,[26] J. Gleason,[16] E. Goetz,[8] R. Goetz,[16] L. Gondan,[82] G. González,[2] N. Gordon,[26] M. L. Gorodetsky,[36] S. Gossan,[62] S. Goßler,[8] R. Gouaty,[3] C. Graef,[8] P. B. Graff,[38] M. Granata,[42] A. Grant,[26] S. Gras,[10] C. Gray,[25] R. J. S. Greenhalgh,[85] A. M. Gretarsson,[86] C. Griffo,[18] P. Groot,[87] H. Grote,[8] K. Grover,[20] S. Grunewald,[21] G. M. Guidi,[45,46] C. Guido,[6] K. E. Gushwa,[1] E. K. Gustafson,[1] R. Gustafson,[57] B. Hall,[43] E. Hall,[1] D. Hammer,[12] G. Hammond,[26] M. Hanke,[8] J. Hanks,[25] C. Hanna,[88] J. Hanson,[6] J. Harms,[1] G. M. Harry,[89] I. W. Harry,[24] E. D. Harstad,[47] M. T. Hartman,[16] K. Haughian,[26] K. Hayama,[83] J. Heefner,[1,*] A. Heidmann,[48] M. Heintze,[16,6] H. Heitmann,[40] P. Hello,[37] G. Hemming,[23] M. Hendry,[26] I. S. Heng,[26] A. W. Heptonstall,[1] M. Heurs,[8] S. Hild,[26] D. Hoak,[52] K. A. Hodge,[1] K. Holt,[6] M. Holtrop,[90] T. Hong,[62] S. Hooper,[39] T. Horrom,[91] D. J. Hosken,[92] J. Hough,[26] E. J. Howell,[39] Y. Hu,[26] Z. Hua,[56] V. Huang,[60] E. A. Huerta,[24] B. Hughey,[86] S. Husa,[53] S. H. Huttner,[26] M. Huynh,[12] T. Huynh-Dinh,[6] J. Iafrate,[2] D. R. Ingram,[25] R. Inta,[64] T. Isogai,[10] A. Ivanov,[1] B. R. Iyer,[93] K. Izumi,[25] M. Jacobson,[1] E. James,[1] H. Jang,[94] Y. J. Jang,[79] P. Jaranowski,[95] F. Jiménez-Forteza,[53] W. W. Johnson,[2] D. Jones,[25] D. I. Jones,[96] R. Jones,[26] R. J. G. Jonker,[9] L. Ju,[39] Haris K.,[97] P. Kalmus,[1] V. Kalogera,[79] S. Kandhasamy,[72] G. Kang,[94] J. B. Kanner,[38] M. Kasprzack,[23,37] R. Kasturi,[98] E. Katsavounidis,[10] W. Katzman,[6] H. Kaufer,[13] K. Kaufman,[62] K. Kawabe,[25] S. Kawamura,[83] F. Kawazoe,[8] F. Kéfélian,[40] D. Keitel,[8] D. B. Kelley,[24] W. Kells,[1] D. G. Keppel,[8]

A. Khalaidovski,[8] F. Y. Khalili,[36] E. A. Khazanov,[99] B. K. Kim,[94] C. Kim,[100,94] K. Kim,[101] N. Kim,[29] W. Kim,[92] Y.-M. Kim,[63] E. J. King,[92] P. J. King,[1] D. L. Kinzel,[6] J. S. Kissel,[10] S. Klimenko,[16] J. Kline,[12] S. Koehlenbeck,[8] K. Kokeyama,[2] V. Kondrashov,[1] S. Koranda,[12] W. Z. Korth,[1] I. Kowalska,[49] D. Kozak,[1] A. Kremin,[72] V. Kringel,[8] A. Królak,[102,103] C. Kucharczyk,[29] S. Kudla,[2] G. Kuehn,[8] A. Kumar,[104] P. Kumar,[24] R. Kumar,[26] R. Kurdyumov,[29] P. Kwee,[10] M. Landry,[25] B. Lantz,[29] S. Larson,[105] P. D. Lasky,[106] C. Lawrie,[26] A. Lazzarini,[1] A. Le Roux,[6] P. Leaci,[21] E. O. Lebigot,[56] C.-H. Lee,[63] H. K. Lee,[101] H. M. Lee,[100] J. Lee,[10] J. Lee,[18] M. Leonardi,[76,77] J. R. Leong,[8] N. Leroy,[37] N. Letendre,[3] B. Levine,[25] J. B. Lewis,[1] V. Lhuillier,[25] T. G. F. Li,[9] A. C. Lin,[29] T. B. Littenberg,[79] V. Litvine,[1] F. Liu,[107] H. Liu,[7] Y. Liu,[56] Z. Liu,[16] D. Lloyd,[1] N. A. Lockerbie,[108] V. Lockett,[18] D. Lodhia,[20] K. Loew,[86] J. Logue,[26] A. L. Lombardi,[52] M. Lorenzini,[59] V. Loriette,[109] M. Lormand,[6] G. Losurdo,[45] J. Lough,[24] J. Luan,[62] M. J. Lubinski,[25] H. Lück,[8,13] A. P. Lundgren,[8] J. Macarthur,[26] E. Macdonald,[7] B. Machenschalk,[8] M. MacInnis,[10] D. M. Macleod,[7] F. Magana-Sandoval,[18] M. Mageswaran,[1] K. Mailand,[1] E. Majorana,[19] I. Maksimovic,[109] V. Malvezzi,[59] N. Man,[40] G. M. Manca,[8] I. Mandel,[20] V. Mandic,[72] V. Mangano,[19,68] M. Mantovani,[14] F. Marchesoni,[44,110] F. Marion,[3] S. Márka,[28] Z. Márka,[28] A. Markosyan,[29] E. Maros,[1] J. Marque,[23] F. Martelli,[45,46] I. W. Martin,[26] R. M. Martin,[16] L. Martinelli,[40] D. Martynov,[1] J. N. Marx,[1] K. Mason,[10] A. Masserot,[3] T. J. Massinger,[24] F. Matichard,[10] L. Matone,[28] R. A. Matzner,[111] N. Mavalvala,[10] G. May,[2] N. Mazumder,[97] G. Mazzolo,[8] R. McCarthy,[25] D. E. McClelland,[64] S. C. McGuire,[112] G. McIntyre,[1] J. McIver,[52] D. Meacher,[40] G. D. Meadors,[57] M. Mehmet,[8] J. Meidam,[9] T. Meier,[13] A. Melatos,[106] G. Mendell,[25] R. A. Mercer,[12] S. Meshkov,[1] C. Messenger,[26] M. S. Meyer,[6] H. Miao,[62] C. Michel,[42] E. E. Mikhailov,[91] L. Milano,[4,54] J. Miller,[64] Y. Minenkov,[59] C. M. F. Mingarelli,[20] S. Mitra,[75] V. P. Mitrofanov,[36] G. Mitselmakher,[16] R. Mittleman,[10] B. Moe,[12] M. Mohan,[23] S. R. P. Mohapatra,[24,58] F. Mokler,[8] D. Moraru,[25] G. Moreno,[25] N. Morgado,[42] T. Mori,[83] S. R. Morriss,[34] K. Mossavi,[8] B. Mours,[3] C. M. Mow-Lowry,[8] C. L. Mueller,[16] G. Mueller,[16] S. Mukherjee,[34] A. Mullavey,[2] J. Munch,[92] D. Murphy,[28] P. G. Murray,[26] A. Mytidis,[16] M. F. Nagy,[74] D. Nanda Kumar,[16] I. Nardecchia,[19,68] T. Nash,[1] L. Naticchioni,[19,68] R. Nayak,[113] V. Necula,[16] G. Nelemans,[87,9] I. Neri,[44,84] M. Neri,[32,33] G. Newton,[26] T. Nguyen,[64] E. Nishida,[83] A. Nishizawa,[83] A. Nitz,[24] F. Nocera,[23] D. Nolting,[6] M. E. Normandin,[34] L. K. Nuttall,[7] E. Ochsner,[12] J. O'Dell,[85] E. Oelker,[10] G. H. Ogin,[1] J. J. Oh,[114] S. H. Oh,[114] F. Ohme,[7] P. Oppermann,[8] B. O'Reilly,[6] W. Ortega Larcher,[34] R. O'Shaughnessy,[12] C. Osthelder,[1] C. D. Ott,[62] D. J. Ottaway,[92] R. S. Ottens,[16] J. Ou,[60] H. Overmier,[6] B. J. Owen,[81] C. Padilla,[18] A. Pai,[97] C. Palomba,[19] Y. Pan,[51] C. Pankow,[12] F. Paoletti,[14,23] R. Paoletti,[14,15] M. A. Papa,[21,12] H. Paris,[25] A. Pasqualetti,[23] R. Passaquieti,[14,30] D. Passuello,[14] M. Pedraza,[1] P. Peiris,[58] S. Penn,[98] A. Perreca,[24] M. Phelps,[1] M. Pichot,[40] M. Pickenpack,[8] F. Piergiovanni,[45,46] V. Pierro,[69] L. Pinard,[42] B. Pindor,[106] I. M. Pinto,[69] M. Pitkin,[26] J. Poeld,[8] R. Poggiani,[14,30] V. Poole,[43] C. Poux,[1] V. Predoi,[7] T. Prestegard,[72] L. R. Price,[1] M. Prijatelj,[8] M. Principe,[69] S. Privitera,[1] G. A. Prodi,[76,77] L. Prokhorov,[36] O. Puncken,[34] M. Punturo,[44] P. Puppo,[19] V. Quetschke,[34] E. Quintero,[1] R. Quitzow-James,[47] F. J. Raab,[25] D. S. Rabeling,[9,50] I. Rácz,[74] H. Radkins,[25] P. Raffai,[28,82] S. Raja,[115] G. Rajalakshmi,[116] M. Rakhmanov,[34] C. Ramet,[6] P. Rapagnani,[19,68] V. Raymond,[1] V. Re,[59,67] C. M. Reed,[25] T. Reed,[117] T. Regimbau,[40] S. Reid,[118] D. H. Reitze,[1,16] F. Ricci,[19,68] R. Riesen,[6] K. Riles,[57] N. A. Robertson,[1,26] F. Robinet,[37] A. Rocchi,[59] S. Roddy,[6] C. Rodriguez,[79] M. Rodruck,[25] C. Roever,[8] L. Rolland,[3] J. G. Rollins,[1] J. D. Romano,[34] R. Romano,[4,5] G. Romanov,[91] J. H. Romie,[6] D. Rosińska,[31,119] S. Rowan,[26] A. Rüdiger,[8] P. Ruggi,[23] K. Ryan,[25] F. Salemi,[8] L. Sammut,[106] V. Sandberg,[25] J. Sanders,[57] V. Sannibale,[1] I. Santiago-Prieto,[26] E. Saracco,[42] B. Sassolas,[42] B. S. Sathyaprakash,[7] P. R. Saulson,[24] R. Savage,[25] R. Schilling,[8] R. Schnabel,[8,13] R. M. S. Schofield,[47] E. Schreiber,[8] D. Schuette,[8] B. Schulz,[8] B. F. Schutz,[21,7] P. Schwinberg,[25] J. Scott,[26] S. M. Scott,[64] F. Seifert,[1] D. Sellers,[6] A. S. Sengupta,[120] D. Sentenac,[23] A. Sergeev,[99] D. Shaddock,[64] S. Shah,[87,9] M. S. Shahriar,[79] M. Shaltev,[8] B. Shapiro,[29] P. Shawhan,[51] D. H. Shoemaker,[10] T. L. Sidery,[20] K. Siellez,[40] X. Siemens,[12] D. Sigg,[25] D. Simakov,[8] A. Singer,[1] L. Singer,[1] A. M. Sintes,[53] G. R. Skelton,[12] B. J. J. Slagmolen,[64] J. Slutsky,[8] J. R. Smith,[18] M. R. Smith,[1] R. J. E. Smith,[20] N. D. Smith-Lefebvre,[1] K. Soden,[12] E. J. Son,[114] B. Sorazu,[26] T. Souradeep,[75] L. Sperandio,[59,67] A. Staley,[28] E. Steinert,[25] J. Steinlechner,[8] S. Steinlechner,[8] S. Steplewski,[43] D. Stevens,[79] A. Stochino,[64] R. Stone,[34] K. A. Strain,[26] N. Straniero,[42] S. Strigin,[36] A. S. Stroeer,[34] R. Sturani,[45,46] A. L. Stuver,[6] T. Z. Summerscales,[121] S. Susmithan,[39] P. J. Sutton,[7] B. Swinkels,[23] G. Szeifert,[82] M. Tacca,[27] D. Talukder,[47] L. Tang,[34] D. B. Tanner,[16] S. P. Tarabrin,[8] R. Taylor,[1] A. P. M. ter Braack,[9] M. P. Thirugnanasambandam,[1] M. Thomas,[6] P. Thomas,[25] K. A. Thorne,[6] K. S. Thorne,[62] E. Thrane,[1,†] V. Tiwari,[16] K. V. Tokmakov,[108] C. Tomlinson,[73] A. Toncelli,[14,30] M. Tonelli,[14,30] O. Torre,[14,15] C. V. Torres,[34] C. I. Torrie,[1,26] F. Travasso,[44,84] G. Traylor,[6] M. Tse,[28] D. Ugolini,[122] C. S. Unnikrishnan,[116] H. Vahlbruch,[13] G. Vajente,[14,30] M. Vallisneri,[62] J. F. J. van den Brand,[9,50] C. Van Den Broeck,[9] S. van der Putten,[9] M. V. van der Sluys,[87,9] J. van Heijningen,[9] A. A. van Veggel,[26] S. Vass,[1] M. Vasúth,[74] R. Vaulin,[10] A. Vecchio,[20] G. Vedovato,[123] J. Veitch,[9] P. J. Veitch,[92] K. Venkateswara,[124] D. Verkindt,[3] S. Verma,[39] F. Vetrano,[45,46] A. Viceré,[45,46] R. Vincent-Finley,[112]

J.-Y. Vinet,[40] S. Vitale,[10,9] B. Vlcek,[12] T. Vo,[25] H. Vocca,[44,84] C. Vorvick,[25] W. D. Vousden,[20] D. Vrinceanu,[34] S. P. Vyachanin,[36] A. Wade,[64] L. Wade,[12] M. Wade,[12] S. J. Waldman,[10] M. Walker,[2] L. Wallace,[1] Y. Wan,[56] J. Wang,[60] M. Wang,[20] X. Wang,[56] A. Wanner,[8] R. L. Ward,[64] M. Was,[8] B. Weaver,[25] L.-W. Wei,[40] M. Weinert,[8] A. J. Weinstein,[1] R. Weiss,[10] T. Welborn,[6] L. Wen,[39] P. Wessels,[8] M. West,[24] T. Westphal,[8] K. Wette,[8] J. T. Whelan,[58] S. E. Whitcomb,[1,39] D. J. White,[73] B. F. Whiting,[16] S. Wibowo,[12] K. Wiesner,[8] C. Wilkinson,[25] L. Williams,[16] R. Williams,[1] T. Williams,[125] J. L. Willis,[126] B. Willke,[8,13] M. Wimmer,[8] L. Winkelmann,[8] W. Winkler,[8] C. C. Wipf,[10] H. Wittel,[8] G. Woan,[26] J. Worden,[25] J. Yablon,[79] I. Yakushin,[6] H. Yamamoto,[1] C. C. Yancey,[51] H. Yang,[62] D. Yeaton-Massey,[1] S. Yoshida,[125] H. Yum,[79] M. Yvert,[3] A. Zadrożny,[103] M. Zanolin,[86] J.-P. Zendri,[123] F. Zhang,[10] L. Zhang,[1] C. Zhao,[39] H. Zhu,[81] X. J. Zhu,[39] N. Zotov,[117,*] M. E. Zucker,[10] and J. Zweizig[1]

[1]*LIGO-California Institute of Technology, Pasadena, California 91125, USA*
[2]*Louisiana State University, Baton Rouge, Louisiana 70803, USA*
[3]*Laboratoire d'Annecy-le-Vieux de Physique des Particules (LAPP), Université de Savoie, CNRS/IN2P3, F-74941 Annecy-le-Vieux, France*
[4]*INFN, Sezione di Napoli, Complesso Universitario di Monte S.Angelo, I-80126 Napoli, Italy*
[5]*Università di Salerno, Fisciano, I-84084 Salerno, Italy*
[6]*LIGO-Livingston Observatory, Livingston, Louisiana 70754, USA*
[7]*Cardiff University, Cardiff, CF24 3AA, United Kingdom*
[8]*Albert-Einstein-Institut, Max-Planck-Institut für Gravitationsphysik, D-30167 Hannover, Germany*
[9]*Nikhef, Science Park, 1098 XG Amsterdam, The Netherlands*
[10]*LIGO-Massachusetts Institute of Technology, Cambridge, Massachusetts 02139, USA*
[11]*Instituto Nacional de Pesquisas Espaciais, 12227-010-São José dos Campos, São Paulo, Brazil*
[12]*University of Wisconsin–Milwaukee, Milwaukee, Wisconsin 53201, USA*
[13]*Leibniz Universität Hannover, D-30167 Hannover, Germany*
[14]*INFN, Sezione di Pisa, I-56127 Pisa, Italy*
[15]*Università di Siena, I-53100 Siena, Italy*
[16]*University of Florida, Gainesville, Florida 32611, USA*
[17]*The University of Mississippi, University, Mississippi 38677, USA*
[18]*California State University Fullerton, Fullerton, California 92831, USA*
[19]*INFN, Sezione di Roma, I-00185 Roma, Italy*
[20]*University of Birmingham, Birmingham, B15 2TT, United Kingdom*
[21]*Albert-Einstein-Institut, Max-Planck-Institut für Gravitationsphysik, D-14476 Golm, Germany*
[22]*Montana State University, Bozeman, Montana 59717, USA*
[23]*European Gravitational Observatory (EGO), I-56021 Cascina, Pisa, Italy*
[24]*Syracuse University, Syracuse, New York 13244, USA*
[25]*LIGO-Hanford Observatory, Richland, Washington 99352, USA*
[26]*SUPA, University of Glasgow, Glasgow, G12 8QQ, United Kingdom*
[27]*APC, AstroParticule et Cosmologie, Université Paris Diderot, CNRS/IN2P3, CEA/Irfu, Observatoire de Paris, Sorbonne Paris Cité, 10, rue Alice Domon et Léonie Duquet, F-75205 Paris Cedex 13, France*
[28]*Columbia University, New York, New York 10027, USA*
[29]*Stanford University, Stanford, California 94305, USA*
[30]*Università di Pisa, I-56127 Pisa, Italy*
[31]*CAMK-PAN, 00-716 Warsaw, Poland*
[32]*INFN, Sezione di Genova, I-16146 Genova, Italy*
[33]*Università degli Studi di Genova, I-16146 Genova, Italy*
[34]*The University of Texas at Brownsville, Brownsville, Texas 78520, USA*
[35]*San Jose State University, San Jose, California 95192, USA*
[36]*Moscow State University, Moscow 119992, Russia*
[37]*LAL, Université Paris-Sud, IN2P3/CNRS, F-91898 Orsay, France*
[38]*NASA/Goddard Space Flight Center, Greenbelt, Maryland 20771, USA*
[39]*University of Western Australia, Crawley, Washington 6009, Australia*
[40]*Université Nice-Sophia-Antipolis, CNRS, Observatoire de la Côte d'Azur, F-06304 Nice, France*
[41]*Institut de Physique de Rennes, CNRS, Université de Rennes 1, F-35042 Rennes, France*
[42]*Laboratoire des Matériaux Avancés (LMA), IN2P3/CNRS, Université de Lyon, F-69622 Villeurbanne, Lyon, France*
[43]*Washington State University, Pullman, Washington 99164, USA*
[44]*INFN, Sezione di Perugia, I-06123 Perugia, Italy*
[45]*INFN, Sezione di Firenze, I-50019 Sesto Fiorentino, Firenze, Italy*
[46]*Università degli Studi di Urbino 'Carlo Bo', I-61029 Urbino, Italy*
[47]*University of Oregon, Eugene, Oregon 97403, USA*
[48]*Laboratoire Kastler Brossel, ENS, CNRS, UPMC, Université Pierre et Marie Curie, F-75005 Paris, France*

[49]*Astronomical Observatory Warsaw University, 00-478 Warsaw, Poland*
[50]*VU University Amsterdam, 1081 HV Amsterdam, The Netherlands*
[51]*University of Maryland, College Park, Maryland 20742, USA*
[52]*University of Massachusetts-Amherst, Amherst, Massachusetts 01003, USA*
[53]*Universitat de les Illes Balears, E-07122 Palma de Mallorca, Spain*
[54]*Università di Napoli 'Federico II', Complesso Universitario di Monte S.Angelo, I-80126 Napoli, Italy*
[55]*Canadian Institute for Theoretical Astrophysics, University of Toronto, Toronto, Ontario M5S 3H8, Canada*
[56]*Tsinghua University, Beijing 100084, China*
[57]*University of Michigan, Ann Arbor, Michigan 48109, USA*
[58]*Rochester Institute of Technology, Rochester, New York 14623, USA*
[59]*INFN, Sezione di Roma Tor Vergata, I-00133 Roma, Italy*
[60]*National Tsing Hua University, Hsinchu Taiwan 300*
[61]*Charles Sturt University, Wagga Wagga, NSW 2678, Australia*
[62]*Caltech-CaRT, Pasadena, California 91125, USA*
[63]*Pusan National University, Busan 609-735, Korea*
[64]*Australian National University, Canberra, ACT 0200, Australia*
[65]*Carleton College, Northfield, Minnesota 55057, USA*
[66]*INFN, Gran Sasso Science Institute, I-67100 L'Aquila, Italy*
[67]*Università di Roma Tor Vergata, I-00133 Roma, Italy*
[68]*Università di Roma 'La Sapienza', I-00185 Roma, Italy*
[69]*University of Sannio at Benevento, I-82100 Benevento, Italy and INFN (Sezione di Napoli), Italy*
[70]*The George Washington University, Washington, District of Columbia 20052, USA*
[71]*University of Cambridge, Cambridge CB2 1TN, United Kingdom*
[72]*University of Minnesota, Minneapolis, Minnesota 55455, USA*
[73]*The University of Sheffield, Sheffield S10 2TN, United Kingdom*
[74]*Wigner RCP, RMKI, H-1121 Budapest, Konkoly Thege Miklós út 29-33, Hungary*
[75]*Inter-University Centre for Astronomy and Astrophysics, Pune-411007, India*
[76]*INFN, Gruppo Collegato di Trento, I-38050 Povo, Trento, Italy*
[77]*Università di Trento, I-38050 Povo, Trento, Italy*
[78]*California Institute of Technology, Pasadena, California 91125, USA*
[79]*Northwestern University, Evanston, Illinois 60208, USA*
[80]*Montclair State University, Montclair, New Jersey 07043, USA*
[81]*The Pennsylvania State University, University Park, Pennsylvania 16802, USA*
[82]*MTA-Eotvos University, 'Lendulet' A. R. G., Budapest 1117, Hungary*
[83]*National Astronomical Observatory of Japan, Tokyo 181-8588, Japan*
[84]*Università di Perugia, I-06123 Perugia, Italy*
[85]*Rutherford Appleton Laboratory, HSIC, Chilton, Didcot, Oxon, OX11 0QX, United Kingdom*
[86]*Embry-Riddle Aeronautical University, Prescott, Arizona 86301, USA*
[87]*Department of Astrophysics/IMAPP, Radboud University Nijmegen, P.O. Box 9010, 6500 GL Nijmegen, The Netherlands*
[88]*Perimeter Institute for Theoretical Physics, Ontario N2L 2Y5, Canada*
[89]*American University, Washington, District of Columbia 20016, USA*
[90]*University of New Hampshire, Durham, New Hampshire 03824, USA*
[91]*College of William and Mary, Williamsburg, Virginia 23187, USA*
[92]*University of Adelaide, Adelaide SA 5005, Australia*
[93]*Raman Research Institute, Bangalore, Karnataka 560080, India*
[94]*Korea Institute of Science and Technology Information, Daejeon 305-806, Korea*
[95]*Białystok University, 15-424 Białystok, Poland*
[96]*University of Southampton, Southampton SO17 1BJ, United Kingdom*
[97]*IISER-TVM, CET Campus, Trivandrum Kerala 695016, India*
[98]*Hobart and William Smith Colleges, Geneva, New York 14456, USA*
[99]*Institute of Applied Physics, Nizhny Novgorod 603950, Russia*
[100]*Seoul National University, Seoul 151-742, Korea*
[101]*Hanyang University, Seoul 133-791, Korea*
[102]*IM-PAN, 00-956 Warsaw, Poland*
[103]*NCBJ, 05-400 Świerk-Otwock, Poland*
[104]*Institute for Plasma Research, Bhat, Gandhinagar 382428, India*
[105]*Utah State University, Logan, Utah 84322, USA*
[106]*The University of Melbourne, Parkville VIC 3010, Australia*
[107]*University of Brussels, Brussels 1050 Belgium*
[108]*SUPA, University of Strathclyde, Glasgow G1 1XQ, United Kingdom*
[109]*ESPCI, CNRS, F-75005 Paris, France*

[110]*Dipartimento di Fisica, Università di Camerino, I-62032 Camerino, Italy*
[111]*The University of Texas at Austin, Austin, Texas 78712, USA*
[112]*Southern University and A&M College, Baton Rouge, Louisiana 70813, USA*
[113]*IISER-Kolkata, Mohanpur, West Bengal 741252, India*
[114]*National Institute for Mathematical Sciences, Daejeon 305-390, Korea*
[115]*RRCAT, Indore MP 452013, India*
[116]*Tata Institute for Fundamental Research, Mumbai 400005, India*
[117]*Louisiana Tech University, Ruston, Louisiana 71272, USA*
[118]*SUPA, University of the West of Scotland, Paisley PA1 2BE, United Kingdom*
[119]*Institute of Astronomy, 65-265 Zielona Góra, Poland*
[120]*Indian Institute of Technology, Gandhinagar Ahmedabad Gujarat 382424, India*
[121]*Andrews University, Berrien Springs, Michigan 49104, USA*
[122]*Trinity University, San Antonio, Texas 78212, USA*
[123]*INFN, Sezione di Padova, I-35131 Padova, Italy*
[124]*University of Washington, Seattle, Washington 98195, USA*
[125]*Southeastern Louisiana University, Hammond, Louisiana 70402, USA*
[126]*Abilene Christian University, Abilene, Texas 79699, USA*
(Received 9 October 2013; published 13 December 2013)

Long gamma-ray bursts (GRBs) have been linked to extreme core-collapse supernovae from massive stars. Gravitational waves (GW) offer a probe of the physics behind long GRBs. We investigate models of long-lived ($\sim$10–1000 s) GW emission associated with the accretion disk of a collapsed star or with its protoneutron star remnant. Using data from LIGO's fifth science run, and GRB triggers from the *Swift* experiment, we perform a search for unmodeled long-lived GW transients. Finding no evidence of GW emission, we place 90% confidence-level upper limits on the GW fluence at Earth from long GRBs for three waveforms inspired by a model of GWs from accretion disk instabilities. These limits range from $F < 3.5$ ergs cm^{-2} to $F < 1200$ ergs cm^{-2}, depending on the GRB and on the model, allowing us to probe optimistic scenarios of GW production out to distances as far as ≈ 33 Mpc. Advanced detectors are expected to achieve strain sensitivities $10\times$ better than initial LIGO, potentially allowing us to probe the engines of the nearest long GRBs.

DOI: 10.1103/PhysRevD.88.122004 PACS numbers: 95.55.Ym

I. INTRODUCTION

Gamma-ray bursts (GRBs) are divided into two classes [1,2]. Short GRBs, lasting $\lesssim 2$ s and characterized by hard spectra, are thought to originate primarily from the merger of binary neutron stars or from the merger of a neutron star with a black hole [3,4]. On the other hand, long GRBs, lasting $\gtrsim 2$ s and characterized by soft spectra, are associated with the extreme core collapse of massive stars [5–8]. In the standard scenario, long GRBs are the product of a relativistic outflow, driven either by a black hole with an accretion disk or a protomagnetar (see, e.g., Refs. [9–12]). At least two types of models have been proposed in which long GRBs may be associated with long-lived $\sim$10–1000 s gravitational-wave (GW) transients. One family of models relies on the formation of clumps in the accretion disk surrounding a newly formed black hole following core collapse [13–17]. The motion of the clumps generates long-lived narrowband GWs.

The second family of models relies on GW emission from a nascent protoneutron star. If the star is born spinning sufficiently rapidly [18], or if it is spun up through fallback accretion [19,20], it may undergo secular or dynamical instabilities [21,22], which, in turn, are expected to produce long-lived narrowband GW transients [20]. Such rapidly spinning protoneutron stars have been invoked to help explain GRB afterglows [18].

The goal of this work is to implement a search for generic long-lived GW transients coincident with long GRBs. While we are motivated by the two families of models discussed above, we make only minimal assumptions about our signal: that it is long-lived and that it is narrowband, producing a narrow track on a frequency-time (ft) map.

Our analysis builds on previous searches for GWs from GRBs by the LIGO [23] and Virgo [24] detectors (see more below). However, this analysis differs significantly from previous LIGO-Virgo GRB analyses [25–29] since previous searches have focused on either short subsecond burst signals or modeled compact binary coalescence signals associated with short GRBs. Here, however, we consider unmodeled signals lasting $\sim$10–1000 s associated with the core-collapse death of massive stars.

During LIGO's fifth science run (S5) (Nov. 5, 2005–Sep. 30, 2007) [23], which provides the data for this analysis, GRBs were recorded by the *Swift* experiment [30] at a rate of ≈ 100 yr^{-1} [31]. GRBs are most commonly detected at distances corresponding to redshifts $z \approx 1$–2 [31],

*Deceased.
†ethrane@ligo.caltech.edu

although nearby GRBs have been detected as close as 37 Mpc [32]. During S5, there were five nearby GRBs (150–610 Mpc) [33]. Unfortunately, LIGO was not observing at the time of these GRBs despite a coincident detector duty cycle of $\approx 50\%$. While none of the GRBs analyzed here are known to be nearby (having a luminosity distance $D_{\text{luminosity}} < 1000$ Mpc and redshift $\lesssim 0.20$), the number of nearby GRBs during S5 bodes well for observing a nearby long GRB coincident with LIGO/Virgo data in the advanced detector era.

The remainder of this paper is organized as follows. In Sec. II we describe the LIGO observatories. In Sec. III we describe the methodology of our search. In Sec. IV we describe the salient features of our signal model. In Sec. V we describe our results and in Sec. VI we discuss implications and future work.

II. THE LIGO OBSERVATORIES

We analyze data from the 4-km H1 and L1 detectors in Hanford, WA and Livingston, LA, respectively. We use data from the S5 science run, during which LIGO achieved a strain sensitivity of $\approx 3 \times 10^{-23}$ Hz$^{-1/2}$ in the most sensitive band between $\sim$100–200 Hz [23]. The H1L1 detector pair provides the most sensitive data available during S5, though a multibaseline approach remains a future goal [34].

S5 saw a number of important milestones (see, e.g., Refs. [35–37]), but most relevant for our present discussion are results constraining the emission of GWs from GRBs [25–28] (see also Ref. [29]). Previous results have limited the distance to long and short GRBs as a function of the available energy for generic waveforms [25,29] and also for compact binary coalescence waveforms [26]. They have investigated the origin of two GRBs that might have occurred in nearby galaxies [27,28].

Currently LIGO [38,39] and Virgo [24] observatories are undergoing major upgrades that are expected to lead to a factor of ten improvement in strain sensitivity, and thus distance reach. The GEO detector [37], meanwhile, continues to take data while the KAGRA detector [40] is under construction. This paper sets the stage for the analysis of long-lasting transients from GRBs in the advanced detector era and demonstrates a long-transient pipeline [41,42] that is expected to have more general applications [20].

III. METHOD

We analyze GRB triggers—obtained through the Gamma-ray burst Coordinates Network [43] and consisting of trigger time, right ascension (RA), and declination (dec)—from the *Swift* satellite's Burst Alert Telescope, which has an angular resolution of $\approx 0.02°$–$0.07°$ [44] which is much smaller than the angular resolution of the GW detector network. This resolution allows us to study GW frequencies up to 1200 Hz while neglecting complications from GRB sky localization errors; see Ref. [42].

LIGO data are preprocessed to exclude corrupt and/or unusable data [45]. In the frequency domain, we remove bins associated with highly nonstationary noise caused by known instrumental artifacts including 60 Hz harmonics and violin resonances [23].

We define a $[-600\text{ s}, +900\text{ s}]$ *on-source* region around each GRB trigger. The GW signal is assumed to exist only in the on-source region. The -600 s allows for possible delays between the formation of a compact remnant object and the emission of the gamma rays (see Ref. [29] and references therein). The $+900$ s is motivated by the hypothesis that GW production is related to GRB afterglows [18], which can extend $\approx$ 10–10^4 s after the initial GRB trigger, though most often the duration is $\lesssim 1000$ s [46,47].

Of the 131 long ($t_{90} > 2$ s) GRB triggers [48] detected by the *Swift* satellite [30] during S5, there are 29 for which coincident H1L1 data are available for the entire 1500 s on-source region. We analyze an additional 21 GRB triggers for which ≥ 1000 s of coincident H1L1 data are available (but not all 1500 s) and hence searchable for signal, although we do not include them in our upper-limit calculations described below.

We additionally require that the GRB is not located in a direction with poor network sensitivity, which can prevent the detection of even a loud signal (see the Appendix for details). Only one GRB is excluded on account of this requirement.

We consider a frequency range of 100–1200 Hz, above which we cannot, at present, probe astrophysically interesting distances due to the increase in detector noise at high frequencies and the fact that strain amplitude falls like $1/f$ for a fixed energy budget. Frequencies $\lesssim 100$ Hz are excluded since nonstationary noise in this band diminishes the sensitivity of the search; see Ref. [42].

Following Ref. [41], strain data from the 1100 Hz $\times$ 1500 s on-source region is converted to spectrograms (ft maps) of strain cross- and auto-power spectra. These ft maps utilize Hann-windowed, 1-s, 50%-overlapping segments with a frequency resolution of 1 Hz (see also Ref. [14]). The strain cross-power is given by [41]

$$\hat{Y}(t;f) \equiv \frac{2}{\mathcal{N}} \text{Re}[Q_{IJ}(t;f,\hat{\Omega})\tilde{s}_I^{\star}(t;f)\tilde{s}_J(t;f)]. \quad (1)$$

Here t is the segment start time, f is the frequency bin, $\mathcal{N}$ is a window normalization factor, $\hat{\Omega}$ is the search direction, and $\tilde{s}_I(t;f)$, $\tilde{s}_J(t;f)$ are discrete Fourier transforms of strain data for segment t using detectors $I = \text{H1}$ and $J = \text{L1}$, respectively. $Q_{IJ}(t;f,\hat{\Omega})$ is a filter function, which takes into account the time delay between the detectors and their directional response (see Ref. [41] for additional details). The dependence of $\hat{Y}(t;f)$ on $\hat{\Omega}$ is implicit for the sake of notational compactness. An estimator for the variance of $\hat{Y}(t;f)$ is given by [41]

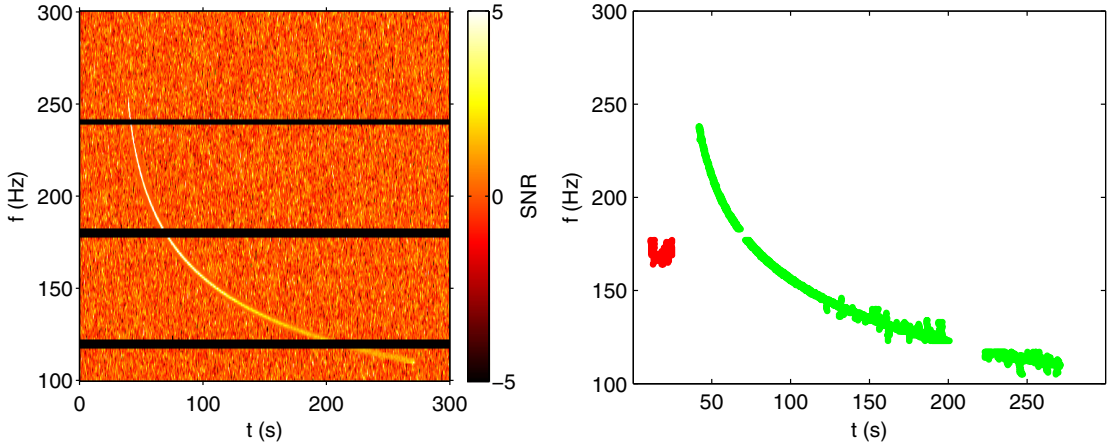

FIG. 1 (color online). Recovery of a simulated waveform in time-shifted noise. Left: ft map of SNR$(t;f)$ for an injected accretion disk instability signal (model c). The horizontal black lines are removed frequency bins corresponding to instrumental artifacts. Right: Significant clusters recovered with the clustering algorithm. Here the green cluster is due to an injected GW signal while the red cluster is due to a noise fluctuation. In this example, the recovered $\mathrm{SNR}_{\mathrm{tot}} = 290$ for the largest cluster (due to the GW signal) is well above the threshold of 30 while noise fluctuations, such as the small red blob shown here, have typical recovered $\mathrm{SNR}_{\mathrm{tot}} = 17$. [Note that the left-hand side color scale shows SNR$(t;f)$, defined in Eq. (3) for each pixel, whereas $\mathrm{SNR}_{\mathrm{tot}}$, defined in Eq. (4), is a property of a cluster consisting of many pixels.]

$$\hat{\sigma}^2(t;f) \equiv \frac{1}{2}|Q_{IJ}(t;f,\hat{\Omega})|^2 P_I'(t;f) P_J'(t;f), \tag{2}$$

where $P_I'(t;f)$ and $P_J'(t;f)$ are the auto-powers measured in detectors I and J, respectively, and the prime denotes that they are calculated using the average of $n = 8$ segments neighboring the one beginning at t (four on each side).

Using Eqs. (1) and (2), we cast our search for long GW transients as a pattern recognition problem (see Fig. 1). GW signals create clusters of positive-valued pixels in ft maps of signal-to-noise ratio (SNR),

$$\mathrm{SNR}(t;f) \equiv \hat{Y}(t;f)/\hat{\sigma}(t;f), \tag{3}$$

whereas noise is randomly distributed with a mean of $\langle \mathrm{SNR}(t;f)\rangle = 0$.

We employ a track-search clustering algorithm for generic narrowband waveforms [49], which works by connecting ft-map pixels above a threshold and that fall within a fixed distance of nearby above-threshold pixels. Clusters (denoted Γ) are ranked by the value of the total cluster signal-to-noise ratio $\mathrm{SNR}_{\mathrm{tot}}$,

$$\mathrm{SNR}_{\mathrm{tot}} = \frac{\sum_{t;f\in\Gamma} \hat{Y}(t;f)\hat{\sigma}^{-2}(t;f)}{\left(\sum_{t;f\in\Gamma} \hat{\sigma}^{-2}(t;f)\right)^{1/2}}. \tag{4}$$

To evaluate the significance of the cluster with the highest $\mathrm{SNR}_{\mathrm{tot}}$ in the on-source region, we compare it to the background distribution, which is estimated using time-shifted data.

Time shifts, in which we offset the H1 and L1 strain series by an amount greater than the intersite GW travel time, provide a robust method of estimating background [50]. For each value of $\mathrm{SNR}_{\mathrm{tot}}$ we assign a false-alarm probability p by performing many trials with time-shifted data (see Fig. 2). The false-alarm probability for $\mathrm{SNR}'_{\mathrm{tot}}$ is given by the fraction of time-shifted trials for which we observed $\mathrm{SNR}_{\mathrm{tot}} \geq \mathrm{SNR}'_{\mathrm{tot}}$. We apply a noise transient identification algorithm [42] in order to mitigate contamination from nonstationary noise. Similar consistency-check noise transient identification is performed in previous searches for unmodeled GW, e.g., Ref. [25]. The relatively good agreement in Fig. 2 between time-shifted and Monte Carlo data (colored Gaussian strain noise) is attributable in part to the

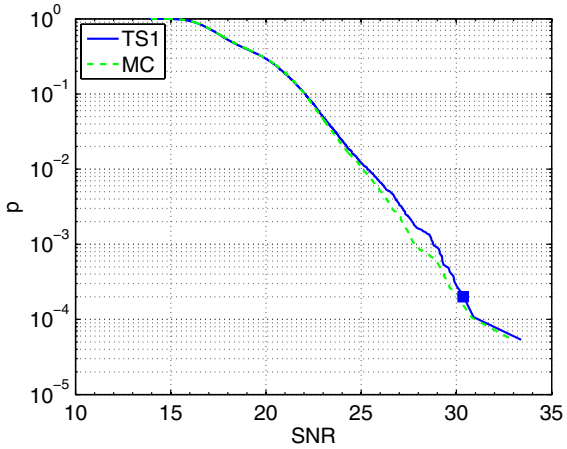

FIG. 2 (color online). Single-trigger false-alarm probability p vs $\mathrm{SNR}_{\mathrm{tot}}$ for time-shifted (TS) and Monte Carlo (MC) data. The marker indicates $\mathrm{SNR}^{\mathrm{th}}_{\mathrm{tot}}$, the threshold for an interesting candidate for follow up. $\mathrm{SNR}^{\mathrm{th}}_{\mathrm{tot}}$ is defined such that the probability of observing any of the 50 GRB triggers with $\mathrm{SNR}_{\mathrm{tot}} > \mathrm{SNR}^{\mathrm{th}}_{\mathrm{tot}}$ due to noise fluctuations is $<1\%$.

stability of LIGO strain noise for frequencies >100 Hz on long time scales [42].

Using time-shifted data, we determine the interesting-candidate threshold $\mathrm{SNR}^{\mathrm{th}}_{\mathrm{tot}}$ such that the probability of observing any of the 50 GRB triggers with $\mathrm{SNR}_{\mathrm{tot}} > \mathrm{SNR}^{\mathrm{th}}_{\mathrm{tot}}$ due to noise fluctuations is <1%. We find that the threshold for an interesting candidate is $\mathrm{SNR}^{\mathrm{th}}_{\mathrm{tot}} = 30$. Interesting candidates, if they are observed, are subjected to further study.

IV. SIGNAL MODELS

In order to constrain physical parameters such as fluence in the absence of a GW detection, it is necessary to have a waveform model. In cases where there is no trusted waveform, one must employ a toy model which is believed to encompass the salient features of the astrophysical phenomenology, such as the sine-Gaussians used in short GW burst analyses [29].

For our toy model, we employ accretion disk instability (ADI) waveforms [51] (based on Refs. [14,15] and references therein) in which a spinning black hole of mass M (with typical values $3M_\odot$–$10M_\odot$) drives turbulence in an accretion torus of mass $m \approx 1.5M_\odot$. This turbulence causes the formation of clumps of mass ϵm (with typical values $0.015M_\odot$–$0.3M_\odot$), the motion of which emits GWs. In optimistic models, as much as $E_{\mathrm{GW}} = 0.1M_\odot c^2$ is emitted in GWs [14]. We emphasize that, like the sine-Gaussian waveforms used in short GW burst analyses, these waveforms should be taken as toy-model representations of a GW signal for which there is significant theoretical uncertainty.

The model is additionally parametrized by a dimensionless spin parameter $a^\star \equiv (c/G)J_{\mathrm{BH}}/M^2$, bounded by $[0, 1)$, where J_{BH} is the angular momentum of the black hole [51]. An ft map of $\mathrm{SNR}(t; f)$ illustrating an injected ADI waveform with parameters $M = 10M_\odot$, $m = 1.5M_\odot$, $\epsilon = 0.04$ and $a^\star = 0.95$ (model c) is shown in the left-hand panel of Fig. 1. (The GW frequency decreases with time as the black hole spins down and the innermost stable circular orbit changes.) The waveforms are calculated assuming a circularly polarized source (inclination angle $\iota \approx 0$), which is a reasonable assumption given that long GRBs are thought to be observed almost parallel to the angular momentum vector [52,53].

TABLE I. Parameters for waveforms [51] inspired by Refs. [14,15]. M is the black hole mass in units of $M_\odot$, $a^\star$ is a dimensionless spin parameter, ϵ is the fraction of torus mass that clumps, and m is the torus mass in units of $M_\odot$. The free parameters (M, $a^\star$, ϵ, m) are selected within the range of expected values in order to produce a range of signal durations.

ID	M	$a^\star$	ϵ	m	t_{dur}	f (Hz)
a	5	0.3	0.05	1.5	39	131–171
b	10	0.95	0.2	1.5	9	90–284
c	10	0.95	0.04	1.5	231	105–259

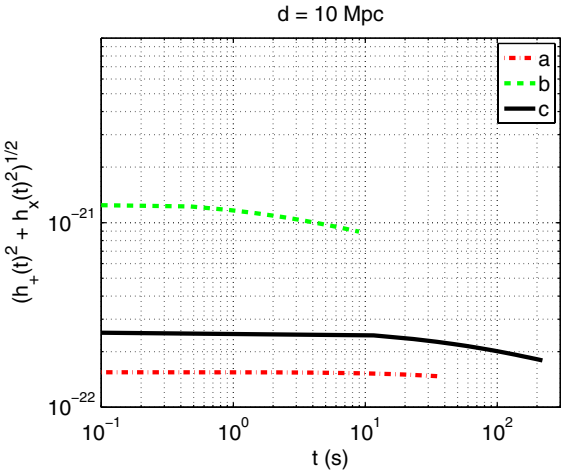

FIG. 3 (color online). Strain amplitude $[h_+^2(t) + h_\times^2(t)]^{1/2}$ vs time for the waveforms in Table I assuming a reference distance of 10 Mpc.

We utilize different combinations of parameters to create three waveforms (denoted a, b, and c), which are summarized in Table I and Fig. 3. By varying the model parameters, we obtain signals of varying durations (9–231 s). For these three waveforms we constrain GW fluence—the GW energy flowing through a unit area at the detector integrated over the emission time. The fluence is defined as

$$F \equiv \frac{c^3}{16\pi G}\int dt(\dot{h}_+^2(t) + \dot{h}_\times^2(t)). \tag{5}$$

By assuming a fixed GW energy budget $E_{\mathrm{GW}} = 0.1M_\odot c^2$, it is possible to cast the fluence limits as limits on the distance D to the GRB. The relationship between fluence, distance, and energy is given by

$$D = \left(\frac{5}{2}\frac{E_{\mathrm{GW}}}{4\pi F}\right)^{1/2}. \tag{6}$$

The factor of $5/2$ arises from the assumption that the source emits face-on, which causes modest enhancement in observed fluence compared to a source observed edge-on.

V. RESULTS

Properties of the loudest cluster for each GRB trigger including its signal-to-noise ratio $\mathrm{SNR}_{\mathrm{tot}}$ and its false-alarm probability p are given in Table II. Of the 50 GRB triggers analyzed in this study, the most significant was GRB 070621 with $\mathrm{SNR}_{\mathrm{tot}} = 24$ corresponding to a single-trigger false-alarm probability of $p = 2.3\%$. The probability of observing $\mathrm{SNR}_{\mathrm{tot}} \geq 24$ among our 50 GRB triggers is 69%.

Since we find no evidence of long-lived GW transients, we set 90% C.L. upper limits on the GW fluence for each GRB trigger for the three test models considered. To calculate these limits we perform pseudoexperiments in which we inject waveforms a, b, and c. All three waveforms are

TABLE II. Swift long GRB triggers coincident with S5 H1L1 data and associated GW search results. "All data?" asks whether there is coincident LIGO data for all 1500s in the on-source region (yes) or for just some of it (no). SNR_{tot} is the signal-to-noise ratio for the loudest cluster and p is the single-trial false alarm probability.

	GRB	GPS	RA (hr)	DEC (deg)	t_{90}(s)	All data?	SNR_{tot}	p (%)
1	GRB060116	821435861	5.65	−5.45	105.9	no	16	89.1
2	GRB060322	827103635	18.28	−36.82	221.5	no	18	49.7
3	GRB060424	829887393	0.49	36.79	37.5	yes	20	27.5
4	GRB060427	830173404	8.28	62.65	64.0	no	16	87.5
5	GRB060428B	830249692	15.69	62.03	57.9	yes	16	85.8
6	GRB060510B	831284548	15.95	78.60	275.2	no	18	55.5
7	GRB060515	831695286	8.49	73.56	52.0	no	18	59.1
8	GRB060516	831797028	4.74	−18.10	161.6	no	17	84.9
9	GRB060607B	833758378	2.80	14.75	31.1	yes	21	21.4
10	GRB060707	836343033	23.80	−17.91	66.2	no	18	46.9
11	GRB060714	836925134	15.19	−6.54	115.0	no	24	3.1
12	GRB060719	837327050	1.23	−48.38	66.9	yes	17	70.0
13	GRB060804	838711713	7.48	−27.23	17.8	no	18	55.2
14	GRB060807	838996909	16.83	31.60	54.0	no	22	10.1
15	GRB060813	839544636	7.46	−29.84	16.1	yes	18	50.7
16	GRB060814	839631753	14.76	20.59	145.3	no	21	16.7
17	GRB060908	841741056	2.12	0.33	19.3	yes	19	43.4
18	GRB060919	842687332	18.46	−50.99	9.1	no	19	43.2
19	GRB060923B	843046700	15.88	−30.91	8.6	no	21	18.3
20	GRB061007	844250902	3.09	−50.50	75.3	yes	18	47.2
21	GRB061021	845480361	9.68	−21.95	46.2	yes	20	30.9
22	GRB061102	846464445	9.89	−17.00	45.6	no	19	43.7
23	GRB061126	848566090	5.77	64.20	70.8	no	22	7.9
24	GRB061202	849082318	7.01	−74.59	91.2	yes	20	32.2
25	GRB061218	850449919	9.95	−35.22	6.5	no	17	75.8
26	GRB061222B	850795876	7.02	−25.86	40.0	yes	21	16.6
27	GRB070107	852206732	10.63	−53.20	347.3	yes	18	53.4
28	GRB070110	852448975	0.06	−52.98	88.4	yes	16	88.4
29	GRB070208	854961048	13.19	61.95	47.7	yes	22	13.0
30	GRB070219	855882630	17.35	69.34	16.6	yes	17	75.6
31	GRB070223	856228514	10.23	43.13	88.5	yes	18	58.2
32	GRB070318	858238150	3.23	−42.95	74.6	yes	20	24.9
33	GRB070330	859330305	17.97	−63.80	9.0	yes	16	95.7
34	GRB070412	860376437	12.10	40.13	33.8	yes	17	74.8
35	GRB070420	861085107	8.08	−45.56	76.5	yes	20	27.5
36	GRB070427	861697882	1.92	−27.60	11.1	yes	19	40.0
37	GRB070506	862464972	23.15	10.71	4.3	yes	21	20.6
38	GRB070508	862633111	20.86	−78.38	20.9	yes	18	48.9
39	GRB070509	862714121	15.86	−78.66	7.7	yes	17	84.6
40	GRB070520B	863718307	8.13	57.59	65.8	no	18	55.7
41	GRB070529	864478122	18.92	20.65	109.2	yes	17	78.6
42	GRB070611	865562247	0.13	−29.76	12.2	yes	22	7.9
43	GRB070612B	865664491	17.45	−8.75	13.5	no	17	77.5
44	GRB070621	866503073	21.59	−24.81	33.3	yes	24	2.3
45	GRB070714B	868424383	3.86	28.29	64.0	yes	19	38.8
46	GRB070721B	869049242	2.21	−2.20	340.0	yes	20	33.3
47	GRB070805	870378959	16.34	−59.96	31.0	yes	17	82.0
48	GRB070911	873525478	1.72	−33.48	162.0	no	18	59.4
49	GRB070917	874049650	19.59	2.42	7.3	no	19	37.7
50	GRB070920B	874357486	0.01	−34.84	20.2	no	22	8.4

TABLE III. Summary of fluence and distance constraints for waveforms a, b, and c. Distance limits are calculated assuming $E_{\rm GW} = 0.1 M_\odot c^2$.

	90% UL on F (ergs cm^{-2}) model			90% LL on D (Mpc) model		
ID	a	b	c	a	b	c
GRB060424	20	25	71	14	12	7.2
GRB060428B	4.9	8.7	21	28	21	13
GRB060607B	94	120	330	6.3	5.7	3.3
GRB060719	20	30	71	14	11	7.3
GRB060813	25	26	74	12	12	7.1
GRB060908	5.6	6.9	20	26	23	14
GRB061007	120	180	620	5.6	4.6	2.5
GRB061021	21	26	89	13	12	6.5
GRB061202	15	22	64	16	13	7.7
GRB061222B	1000	80	280	1.9	6.8	3.7
GRB070107	270	410	1200	3.7	3.0	1.8
GRB070110	6.7	8.3	29	24	21	11
GRB070208	4.4	5.5	16	29	26	15
GRB070219	14	21	59	16	14	8.0
GRB070223	13	16	47	17	15	8.9
GRB070318	4.9	6.1	21	28	25	13
GRB070330	3.7	5.5	16	32	26	15
GRB070412	5.9	8.8	25	25	21	12
GRB070420	25	22	74	12	13	7.1
GRB070427	4.4	5.5	16	29	26	15
GRB070506	15	22	54	16	13	8.4
GRB070508	6.1	9.1	26	25	20	12
GRB070509	7.9	12	34	22	18	11
GRB070529	9.0	11	32	20	18	11
GRB070611	3.5	4.4	15	33	29	16
GRB070621	4.6	4.7	16	29	28	15
GRB070714B	46	69	160	9.0	7.4	4.8
GRB070721B	9.6	14	41	20	16	9.6
GRB070805	8.0	14	34	22	16	10

normalized to a fixed energy budget $E_{\rm GW} = 0.1 M_\odot$ by multiplying each strain time series by a constant [54]. We vary the distance to the source in order to determine the distance for which 90% of the injected signals are recovered with an $\mathrm{SNR}_{\rm tot}$ exceeding the loudest cluster in the on-source region. From these distance limits, we obtain fluence limits from Eq. (6).

GW strain measurements are subject to systematic calibration uncertainties. For S5 H1,L1 and for $f < 2000$ Hz, this error is estimated to be 10.4%, 14.4% in amplitude [55]. In order to take calibration error into account in our upper limit calculation, we assume the true fluence is some number λ times the measured fluence, and that λ is Gaussian distributed with a mean of 1 and a width of $\sqrt{10.4\%^2 + 14.4\%^2} = 17.8\%$. Marginalizing over λ leads to a 15% reduction in our distance sensitivity. Phase and timing calibration errors are negligible for this analysis [55].

The 90% C.L. limits for models a, b, and c are reported in Table III. We report upper limits (UL) on fluence and lower limits (LL) on distance assuming a GW energy budget of $E_{\rm GW} = 0.1 M_\odot c^2$. For model a, we place upper limits on GW fluence of 3.5–1000 ergs cm^{-2} (corresponding to distance lower limits of 1.9–33 Mpc). For model b, the corresponding limits are $F < 4.4$–410 ergs cm^{-2} ($D > 3.0$–29 Mpc), and for model c, $F < 16$–1200 ergs cm^{-2} ($D > 1.8$–15 Mpc). The variation in limits for a given model is due primarily to the direction-dependent antenna response factors, which cause $\sigma(t; f)$ to vary by two orders of magnitude for different search directions. The GRB for which we set the best limits is GRB 070611 while the least sensitive limits are placed on GRB 070107.

Given a fixed waveform with an overall normalization constant, fluence limits are proportional to limits on (the square of) the root-sum-squared strain,

$$h_{\rm rss}^2 \equiv \int dt (h_+^2(t) + h_\times^2(t)) = kF, \tag{7}$$

where k is a waveform-dependent constant. Using this relation, we can alternatively present the limits as

$$h^a_{\rm rss} < 7.0 \times 10^{-22} (F/3.5\ {\rm erg\,cm^{-2}})^{1/2},$$
$$h^b_{\rm rss} < 7.7 \times 10^{-22} (F/4.4\ {\rm erg\,cm^{-2}})^{1/2}, \quad (8)$$
$$h^c_{\rm rss} < 1.5 \times 10^{-21} (F/16\ {\rm erg\,cm^{-2}})^{1/2}.$$

The superscript of $h_{\rm rss}$ refers to the different models.

VI. IMPLICATIONS AND FUTURE WORK

In the most optimistic scenarios for the production of GWs in stellar collapse, it has been claimed that as much as $E_{\rm GW} = 0.1 M_\odot c^2$ of energy is converted into GWs [14]. The GW signature from the actual core collapse, as opposed to subsequent emission from an accretion disk or from a protoneutron star remnant, is expected to be significantly less energetic, with a typical energy budget of $E_{\rm GW} = \sim 10^{-11}$–$10^{-7} M_\odot$ [56].

By comparing our best fluence upper limits $F^{90\%} = 3.5\ {\rm ergs\,cm^{-2}}$ (GRB070611, model *a*) with this prediction, we extrapolate approximate distance lower limits as a function of frequency for this best-case scenario; see Fig. 4. In the most sensitive frequency range between 100–200 Hz, the limits are as large as $D^{90\%} = 33$ Mpc. They fall like $D^{90\%} \propto f^{-2}$ above 200 Hz due to increasing the detector shot noise as well as from the relationship between energy and strain $E_{\rm GW} \propto f^2 h^2$. The limits in Fig. 4 scale like $D^{90\%} \propto E_{\rm GW}^{1/2}$ and $D^{90\%} \propto (F^{90\%})^{-1/2}$. The GW power spectral peak frequency is marked with a red circle. Note that the waveforms we consider here are not characterized by a single frequency, and so Fig. 4 should be taken as an approximate indicator of how results scale with frequency.

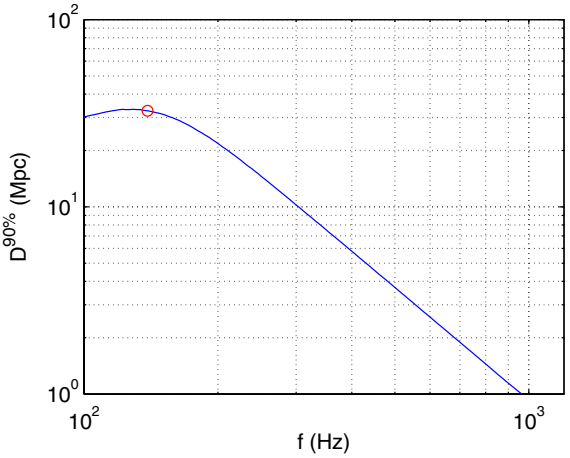

FIG. 4 (color online). Best-case-scenario, approximate 90% C.L. lower limits on the distance to sources of long-lived GW transients extrapolated from fluence upper limits. Following Ref. [14], we assume a GW energy budget of $0.1 M_\odot c^2$. The limits are calculated using the best fluence constraints from Table III: $F^{90\%} = 3.5\ {\rm ergs\,cm^{-2}}$ from GRB070611, model *a*. The GW power spectral peak is marked with a red circle. The frequency dependence should be taken as indicating an approximate trend as our waveforms are not monochromatic. Also, the extrapolation assumes a smooth detector noise curve, which only approximates the LIGO detector noise.

If the GW frequency is high ($f \gtrsim 1$ kHz) [14], the reach of initial LIGO is only $\lesssim 1$ Mpc due to the fact that distance sensitivity falls off rapidly with frequency: $D \propto f^{-2}$. The nearest GRB in our set with a known redshift measurement, GRB 070420, is estimated to have occurred at $z = 0.48$–0.93 ($D_{\rm luminosity} = 2800$–$6400$ Mpc) [57], well beyond our exclusion distances even for lower-frequency emission.

While we are therefore unable to rule out the most extreme models of GW emission with the present analysis, we have demonstrated that initial LIGO can test optimistic models out to distances as far as ≈ 33 Mpc depending on the GW frequency and the detector orientation during the time of the GRB. Advanced LIGO and Advanced Virgo are expected to achieve strain sensitivities $10\times$ better than the initial LIGO data analyzed here, which will be sufficient to test extreme models out to $D \approx 330$ Mpc. As discussed in Sec. I, GRBs are not infrequent at such distances [58].

Meanwhile, work is ongoing to develop more sophisticated data analysis procedures, to further enhance sensitivity. By tuning our analysis pipeline [41] for long-lived signals, we estimate that we can detect ADI waveforms for sources that are twice as distant as could have been detected by previous searches tuned for short signals [25,29] (corresponding to an increase in detection volume of $\approx 8\times$). In order to achieve additional improvements in sensitivity, work is ongoing to explore alternative pattern recognition strategies that relax the requirement that ${\rm SNR}(t; f)$ exceeds some threshold to form a pixel cluster [see Eq. (3)].

Long GRBs are by no means the only interesting source of long GW transients. In Refs. [19,20] it was argued that core-collapse supernovae can trigger the production of long-lived GW emission through fallback accretion. While the predicted strains are much less than the most extreme models considered here, the local rate of supernovae is much higher than the local rate of long GRBs, and preliminary sensitivity estimates suggest that fallback accretion-powered signals are interesting targets for Advanced LIGO/Virgo [20]. Other scenarios for long-lived GW production explored in Ref. [41], including protoneutron star convection and eccentric black hole binaries, remain areas of investigation. This analysis paves the way for future studies probing unmodeled long-lived GW emission.

ACKNOWLEDGMENTS

The authors gratefully acknowledge the support of the United States National Science Foundation for the construction and operation of the LIGO Laboratory, the Science and Technology Facilities Council of the United Kingdom, the Max-Planck-Society, and the State of Niedersachsen/Germany for support of the construction and operation of the GEO600 detector, and the Italian

Istituto Nazionale di Fisica Nucleare and the French Centre National de la Recherche Scientifique for the construction and operation of the Virgo detector. The authors also gratefully acknowledge the support of the research by these agencies and by the Australian Research Council, the International Science Linkages program of the Commonwealth of Australia, the Council of Scientific and Industrial Research of India, the Istituto Nazionale di Fisica Nucleare of Italy, the Spanish Ministerio de Economía y Competitividad, the Conselleria d'Economia Hisenda i Innovació of the Govern de les Illes Balears, the Foundation for Fundamental Research on Matter supported by the Netherlands Organisation for Scientific Research, the Polish Ministry of Science and Higher Education, the FOCUS Programme of Foundation for Polish Science, the Royal Society, the Scottish Funding Council, the Scottish Universities Physics Alliance, The National Aeronautics and Space Administration, OTKA of Hungary, the Lyon Institute of Origins (LIO), the National Research Foundation of Korea, Industry Canada and the Province of Ontario through the Ministry of Economic Development and Innovation, the National Science and Engineering Research Council Canada, the Carnegie Trust, the Leverhulme Trust, the David and Lucile Packard Foundation, the Research Corporation, and the Alfred P. Sloan Foundation.

APPENDIX: DIRECTIONAL SENSITIVITY CUT

The pipeline used in this analysis works by comparing $\hat{Y}(t;f)$ [Eq. (1)] to $\sigma(t;f)$ [Eq. (2)], which depends on the auto-power in the four neighboring segments on each side of t (for additional details see Ref. [41]). For a fixed direction on the sky $\hat{\Omega}$, the expectation value of $\mathrm{SNR}(t;f) \equiv \hat{Y}(t;f)/\sigma(t;f)$ for one such pixel depends on the "pair efficiency" ϵ_{IJ} for each detector pair,

$$\langle \mathrm{SNR}(t;f)\rangle \propto \frac{\epsilon_{12}(t;\hat{\Omega})}{[\epsilon_{11}(t;\hat{\Omega})\epsilon_{22}(t;\hat{\Omega})]^{1/2}}. \tag{A1}$$

Pair efficiency is defined in terms of the antenna response factors (see, e.g., Ref. [41]),

$$\epsilon_{IJ}(t;\hat{\Omega}) \equiv \frac{1}{2}\sum_{A} F_I^A(t,\hat{\Omega})F_J^A(t,\hat{\Omega}). \tag{A2}$$

For a small subset of directions $\hat{\Omega}$, the following condition is met:

$$\epsilon_{12} \ll (\epsilon_{11}(t;\hat{\Omega})\epsilon_{22}(t;\hat{\Omega}))^{1/2}, \tag{A3}$$

which means the GW signal produces a much stronger auto-power spectra compared to the cross-power spectra. In the most extreme cases, the GW signal in the segments neighboring t causes $\sigma(t;f) \gg \hat{Y}(t;f)$, which makes $\mathrm{SNR}(t;f) \approx 0$ even for loud signals.

To avoid searching in directions for which we are blind to GWs and can therefore not set limits, we employ a cut that ensures that GW signals can produce seed pixels with $\mathrm{SNR}(t;f) \gtrsim 1$,

$$\epsilon_{12} \geq \frac{1}{4}(\epsilon_{11}(t;\hat{\Omega})\epsilon_{22}(t;\hat{\Omega}))^{1/2}. \tag{A4}$$

We find that this cut eliminates GRB triggers for which we cannot set effective limits while removing only one out of 51 GRB triggers.

[1] C. Kouveliotou, C. A. Meegan, G. J. Fishman, N. P. Bhat, M. S. Briggs, T. M. Koshut, W. S. Paciesas, and G. N. Pendleton, Astrophys. J. Lett. **413**, L101 (1993).
[2] N. Gehrels *et al.*, Nature (London) **444**, 1044 (2006).
[3] D. Eichler, M. Livio, T. Piran, and D. N. Schramm, Nature (London) **340**, 126 (1989).
[4] R. Mochkovitch, M. Hernanz, J. Isern, and X. Martin, Nature (London) **361**, 236 (1993).
[5] S. Campana *et al.*, Nature (London) **442**, 1008 (2006).
[6] E. Pian *et al.*, Nature (London) **442**, 1011 (2006).
[7] A. M. Soderberg *et al.*, Nature (London) **442**, 1014 (2006).
[8] P. A. Mazzali, J. Deng, K. Nomoto, D. N. Sauer, E. Pian, N. Tominaga, M. Tanaka, K. Maeda, and A. V. Filippenko, Nature (London) **442**, 1018 (2006).
[9] C. Thompson, Mon. Not. R. Astron. Soc. **270**, 480 (1994).
[10] A. I. MacFadyen, S. E. Woosley, and A. Heger, Astrophys. J. **550**, 410 (2001).
[11] S. E. Woosley, Astrophys. J. **405**, 273 (1993).
[12] B. Paczyński, Astrophys. J. Lett. **494**, L45 (1998).
[13] A. L. Piro and E. Pfahl, Astrophys. J. **658**, 1173 (2007).
[14] M. H. P. M. van Putten, Phys. Rev. Lett. **87**, 091101 (2001).
[15] M. H. P. M. van Putten, Astrophys. J. Lett. **684**, L91 (2008).
[16] I. A. Bonnell and J. E. Pringle, Mon. Not. R. Astron. Soc. **273**, L12 (1995).
[17] K. Kiuchi, M. Shibata, P. J. Montero, and J. A. Font, Phys. Rev. Lett. **106**, 251102 (2011).
[18] A. Corsi and P. Mészáros, Astrophys. J. **702**, 1171 (2009).
[19] A. L. Piro and C. D. Ott, Astrophys. J. **736**, 108 (2011).
[20] A. L. Piro and E. Thrane, Astrophys. J. **761**, 63 (2012).
[21] S. Chandrasekhar, *The Silliman Foundation Lectures* (*Yale University Press*, New Haven, 1969).
[22] B. Owen and L. Lindblom, Classical Quantum Gravity **19**, 1247 (2002).
[23] B. P. Abbott *et al.*, Rep. Prog. Phys. **72**, 076901 (2009).
[24] F. Acernese (Virgo Collaboration), Classical Quantum Gravity **23**, S63 (2006).

[25] B. P. Abbott *et al.*, Astrophys. J. **715**, 1438 (2010).
[26] J. Abadie *et al.*, Astrophys. J. **715**, 1453 (2010).
[27] J. Abadie *et al.*, Astrophys. J. **755**, 2 (2012).
[28] B. Abbott *et al.*, Astrophys. J. **681**, 1419 (2008).
[29] J. Abadie *et al.*, Astrophys. J. **760**, 12 (2012).
[30] N. Gehrels *et al.*, Astrophys. J. **611**, 1005 (2004).
[31] N. Gehrels, E. Ramirez-Ruiz, and D. B. Fox, Annu. Rev. Astron. Astrophys. **47**, 567 (2009).
[32] T. J. Galama *et al.*, Nature (London) **395**, 670 (1998).
[33] Here we assume a Hubble parameter $H_0 = 67.8\ \mathrm{km\,s^{-1}\,Mpc^{-1}}$ and matter energy density $\Omega_m = 0.27$.
[34] By adding additional detectors to the network (and computational complexity to the pipeline), it is possible to further improve sensitivity, though, for most GRBs, the gain for this analysis is expected to be marginal since the sensitivity is dominated by the most sensitive detector pair.
[35] B. Abbott *et al.*, Astrophys. J. Lett. **683**, L45 (2008).
[36] B. Abbott *et al.*, Nature (London) **460**, 990 (2009).
[37] H. Grote and the (LIGO Scientific Collaboration), Classical Quantum Gravity **27**, 084003 (2010).
[38] G. M. Harry (LIGO Scientific Collaboration), Classical Quantum Gravity **27**, 084006 (2010).
[39] B. Iyer *et al.*, lIGO-India Tech. rep. https://dcc.ligo.org/cgi-bin/DocDB/ShowDocument?docid=75988.
[40] K. Kuroda, Classical Quantum Gravity **27**, 084004 (2010).
[41] E. Thrane *et al.*, Phys. Rev. D **83**, 083004 (2011).
[42] T. Prestegard, E. Thrane, N. L. Christensen, M. W. Coughlin, B. Hubbert, S. Kandhasamy, E. MacAyeal, and V. Mandic, Classical Quantum Gravity **29**, 095018 (2012).
[43] GCN, http://gcn.gsfc.nasa.gov.
[44] NASA Goddard Space Flight Center, http://heasarc.nasa.gov/docs/swift/archive/grb_table/.
[45] L. Blackburn *et al.*, Classical Quantum Gravity **25**, 184004 (2008).
[46] A. Panaitescu and W. T. Vestrand, Mon. Not. R. Astron. Soc. **387**, 497 (2008).
[47] A search exploring times as long as 10^4 s after the GRB trigger presents additional computational burdens, and is therefore beyond our present scope.
[48] The t_{90} time is defined as the duration in between the 5% and 95% total background-subtracted photon counts.
[49] T. Prestegard and E. Thrane, LIGO DCC #L1200204 https://dcc.ligo.org/cgi-bin/DocDB/ShowDocument?docid=93146.
[50] B. Abbott *et al.*, Phys. Rev. D **69**, 122001 (2004).
[51] L. Santamaría and C. D. Ott, LIGO DCC p. T1100093 (2011), https://dcc.ligo.org/LIGO-T1100093-v2/public.
[52] A. Gal-Yam, E. O. Ofek, D. Poznanski, A. Levinson, E. Waxman, D. A. Frail, A. M. Soderberg, E. Nakar, W. Li, and A. V. Filippenko, Astrophys. J. **639**, 331 (2006).
[53] J. L. Racusin, E. W. Liang, D. N. Burrows, A. Falcone, T. Sakamoto, B. B. Zhang, B. Zhang, P. Evans, and J. Osborne, Astrophys. J. **698**, 43 (2009).
[54] In reality, E_{GW} depends on model parameters, but it is useful for our present purposes to normalize all three waveforms to the same energy in order to observe how sensitivity varies with signal duration and morphology.
[55] J. Abadie *et al.*, Nucl. Instrum. Methods Phys. Res., Sect. A **624**, 223 (2010).
[56] C. Ott, Classical Quantum Gravity **26**, 063001 (2009).
[57] L. Xiao and B. E. Schaefer, Astrophys. J. **731**, 103 (2011).
[58] Given a GRB rate of $\approx 0.5\ \mathrm{Gpc^{-3}\,yr^{-1}}$ and a detection volume of $(4\pi/3)(0.33\ \mathrm{Gpc})^3$, we expect an event rate of $\approx 0.1\ \mathrm{yr^{-1}}$, though the local rate is actually somewhat higher.